Stability thresholds and calculation techniques for fast entangling gates on trapped ions

C. D. B. Bentley,[1,*] R. L. Taylor,[1] A. R. R. Carvalho,[1,2] and J. J. Hope[1]

[1]*Department of Quantum Science, Research School of Physics and Engineering, The Australian National University, Canberra, ACT 2601, Australia*

[2]*Centre for Quantum Computation and Communication Technology, Department of Quantum Science, Research School of Physics and Engineering, The Australian National University, Canberra, ACT 2601, Australia*

(Received 12 January 2016; published 28 April 2016)

Fast entangling gates have been proposed for trapped ions that are orders of magnitude faster than current implementations. We present here a detailed analysis of the challenges involved in performing a successful fast gate. We show that the rotating wave approximation is stable with respect to pulse numbers: the time scale on which we can neglect terms rotating at the atomic frequency is negligibly affected by the number of pulses in the fast gate. In contrast, we show that the laser pulse instability does give rise to a pulse-number-dependent effect; the fast gate infidelity is compounded with the number of applied imperfect pulses. Using the dimensional reduction method presented here, we find bounds on the pulse stability required to achieve two-qubit gate fidelity thresholds.

DOI: 10.1103/PhysRevA.93.042342

I. INTRODUCTION

A two-qubit entangling gate is an essential component of any quantum information processing (QIP) system [1]. Fast gates for trapped ions using controlled large momentum kicks offer a significantly faster operation time scale than traditional gates requiring spectral resolution of sidebands [2–7]. This in turn leads to simpler gate adaption for long ion crystals or more complex geometries [3,8–10], such that sufficiently fast two-qubit gate schemes for two trapped ions require only minimal adaption to be directly applied to longer crystals with a high fidelity [6,11]. There has been recent progress towards the implementation of pulsed fast gates: the required high-repetition-rate pulsed lasers have been produced [12] and used to perform a single-qubit gate [13], as well as spin-motion entanglement [14]. In this paper we outline challenges to performing a complete fast gate protocol and present both the techniques for quantifying gate fidelity subject to imperfections and the required thresholds of laser stability and pulse times to perform high-fidelity gates.

For implementation of a fast gate, and certainly for consideration of their application to large-scale algorithms, detailed analysis of the stability requirements for the trap and control is critical. Error correction can be applied between gate operations, however, individual gate operations are required to meet high-fidelity thresholds [15–17]. The scheme proposed by García-Ripoll, Zoller, and Cirac (GZC) [2] and the fast robust antisymmetric gate (FRAG scheme) [5] were shown in [6] to have a very high fidelity and robustness, and we focus on these schemes for our error analysis. While perfect GZC and FRAG gates are independent of the initial motional states, errors in the gate are enhanced according to the mean vibrational mode occupation, as shown in [4,6]. Certain gate error sources have been considered: the effects of trap anharmonicity on both schemes [2,4,6], dissipation effects on the GZC scheme [4], and laser control errors in the FRAG scheme such as insufficient laser repetition rates and pulse timing or direction errors [5]. Only a preliminary analysis of pulsed fast gate errors due to pulse area imperfections has been performed, despite the conclusion that such errors are significant [2,5]. Furthermore, a phase stability analysis is still required.

Laser phase dependence in each momentum kick comprising the fast gates arises when the rotating wave approximation (RWA) is no longer valid due to short pulse durations relative to the atomic transition frequency. This leads to imperfect population transfer between internal states. Short pulse durations are necessary such that the total motional evolution during the pulses is negligible. Thus the combined duration from all of the applied pulses is required to be much shorter than the trap period, which is of the order of 1 μs. Few pulses or very short pulse durations seem preferable, however, increasing the number of pulse pairs in a fast gate improves the gate speed, fidelity, and scaling with the number of ions. The RWA provides the lower bound for pulse durations for fast gates, and examining the dependence of this lower bound on the number of pulses in a gate is essential for applications of fast gates to QIP.

Significant infidelity also arises from imperfect applied pulses. Ideal pulses keep the internal qubit states invariant throughout the phase gate and restore the initial motional state at the end of the gate, however, imperfect pulses cause internal state transfers as well as the occupation of a range of motional levels after the gate. Random errors in the pulse duration were considered in [2] for a four-kick sequence, and in [5] a worst-case error bound was calculated using perturbation theory for small errors in the pulse area and low numbers of pulse pairs. The perturbation technique was used for just four pulse pairs and fails well before 100 pulse pairs, with an error of the order of 1% in the pulse area [5]. It was concluded that an imperfect pulse area will limit the fidelity of fast gates; a more complete analysis of the required pulse stability is necessary for gate implementation.

It is possible to model the full dynamics of a gate without the RWA or with pulse area imperfections and, thereby, directly calculate the gate fidelity. However, the Hamiltonian operator required for this calculation has a dimension given by the square of the full state vector dimension, which includes both the internal qubit states and the vibrational mode states for each shared mode. In the ideal-pulse case, the complexity is vastly reduced by simplifying the requirements for performing

*christopher.bentley@anu.edu.au

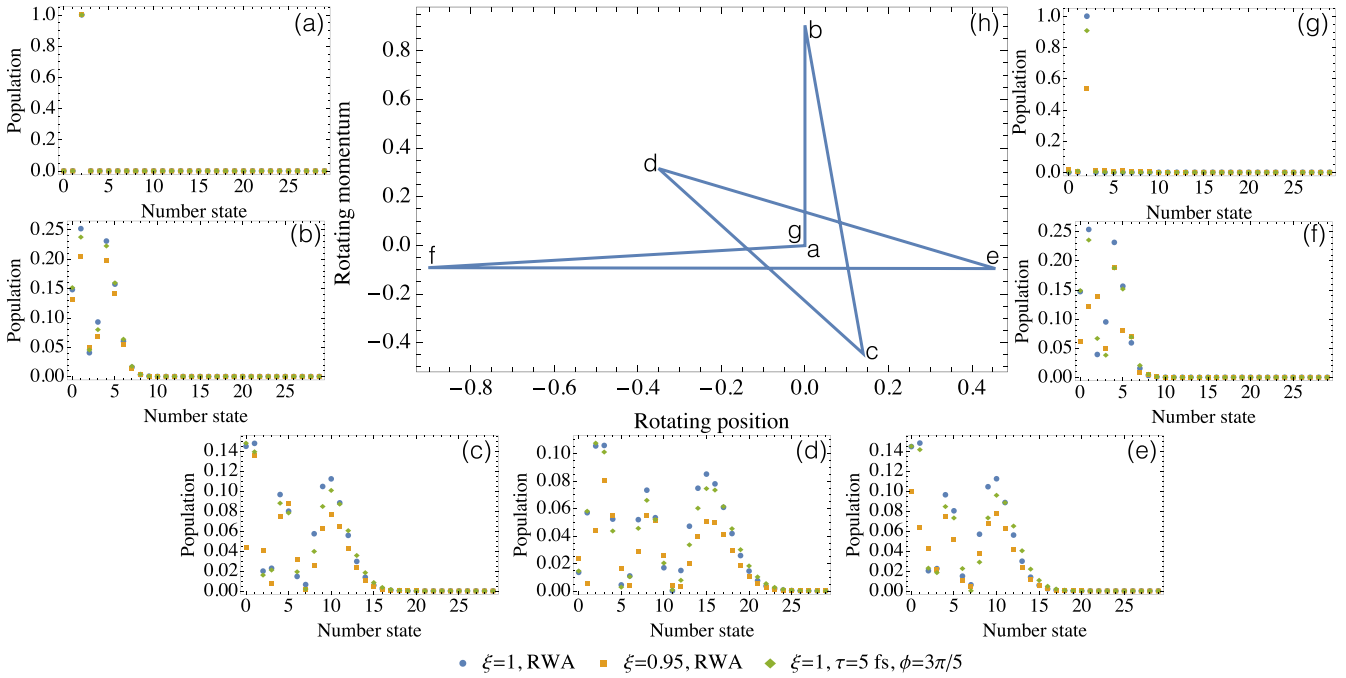

FIG. 1. (h) Center-of-mass (c.m.) phase-space trajectory for the center of a coherent state during the gate operation. The sides of the trajectory correspond to momentum kicks. The angle of each vertex corresponds to free evolution between kicks and marks the gate evolution point for the other figures, from (a) to (g). (a–g) Population occupying c.m. mode number states, for both ions in the excited state, at different points during the GZC gate operation, with $n = 1$ (14 total pulse pairs). Blue circles represent an ideal gate, satisfying the rotating wave approximation (RWA) and with no pulse area imperfections given by $(1 - \xi)$. A gate with systematic pulse imperfections ($\xi = 0.95$) is also considered (yellow squares), as well as a gate where the RWA is invalid (green diamonds) such that the pulse duration and laser phase must be defined ($\tau = 5$ fs, $\phi = 3\pi/5$). After the nonideal gates, population is lost to other internal states, and some of the population is imperfectly restored to the initial c.m. state, $|2\rangle_c$, the second excited number state. Values were chosen to illustrate the effects of these errors. The point in the gate operation described by (a)–(g) corresponds to a–g in (h).

a high-fidelity gate to three control conditions [2]. In this paper, we present a simplification method for imperfect gates that permits fidelity calculation for large momentum kicks in traps with many ions and a corresponding number of shared motional modes. Our method is presented in Sec. II following a review of fast gates. In Sec. III, we apply this fidelity calculation technique to explore the effect of pulse number on the phase dependence of the gate with short pulse durations. This provides a minimum pulse duration bound for high-fidelity fast gates composed of varying numbers of pulses. In Sec. IV, we apply our method to consideration of imperfect pulse areas comprehensively. We introduce the errors in the atom-light evolution unitaries and construct the imperfect gate evolution operators to directly compute the fidelity. This gives us an accurate measure of fidelity for large numbers of pulses. Finally, we present our conclusions in Sec. V.

II. QUANTIFYING FAST GATE ERRORS

We present the fast gate mechanism and summarize the GZC and FRAG gate schemes, followed by a general fidelity calculation method for two trapped ions as well as a two-ion gate in a longer ion crystal.

A. Gate dynamics and limitations

Fast gates operate in the strong-coupling regime, where the laser coupling is much greater than the trap frequency, $\Omega \gg \nu$. In this regime, multiple number states of each shared motional mode are excited by pairs of counter-propagating laser pulses, as shown in Fig. 1. These π-pulse pairs provide momentum kicks such that a closed trajectory in phase space is described for the center of a coherent state, as in Fig. 1(h). The area enclosed in each mode's phase space determines a conditional phase applied to different two-qubit computational states.

The evolution of an ideal fast gate can be described as alternating displacement and rotation operators in phase space for each motional mode. A displacement operator for mode p is described by

$$\hat{D}_p(\alpha) = \exp[\alpha a_p^\dagger - \alpha^* a_p], \tag{1}$$

for a displacement of α, where a_p is the mode annihilation operator. Under the RWA, pairs of counter-propagating π pulses give rise to mode displacement operators as follows [6]:

$$U_{\text{kick}} = e^{-2izk(x_1\sigma_1^z + x_2\sigma_2^z)} \tag{2}$$

$$= \Pi_{p=1}^{L} \hat{D}_p\big(-2iz(b_1^{(p)}\sigma_1^z + b_2^{(p)}\sigma_2^z)\eta_p\big), \tag{3}$$

when there is negligible motional evolution between the two pulses. Here z is the direction of the first pulse in the pair, k is the laser wave number, x_i is the position operator for ion i, and σ_i^z is the usual Pauli Z operator acting on ion i. There are L motional modes corresponding to L ions in the crystal, and $b_i^{(p)}$ is the ion-mode coupling coefficient between ion i and mode

p. The Lamb-Dicke parameter η_p for mode p is given by

$$\eta_p = k\sqrt{\frac{\hbar}{2M\nu_p}} \tag{4}$$

for ion mass M and mode frequency ν_p.

Two main causes of imperfect momentum kicks to the ions come from counter-propagating pulses applied with an area not equal to π or from breaking the RWA through short pulse durations. These imperfections are shown in Fig. 1, which illustrates their effect at each stage in the fast gate evolution process.

The free motion of the ions (and their motional modes) corresponds to rotation operators in each mode p's phase space,

$$U_{p,\mathrm{mot}} = e^{-i\nu_p \delta t_k a_p^\dagger a_p}, \tag{5}$$

where δt_k is the time between the kth and the $(k+1)$th momentum kicks.

The displacements and free rotations are determined according to particular pulse schemes. These schemes satisfy the required gate conditions: (i) conditional phase evolution according to the two-qubit gate described by

$$U_{\mathrm{gate}} = e^{i\frac{\pi}{4}\sigma_1^z\sigma_2^z} \tag{6}$$

for a gate applied to ions 1 and 2, and (ii) no motional dependence, such that the initial motional state is restored following the gate operation. The GZC and FRAG schemes are characterized by pulse pairs z applied at times t, interspersed with free evolution. For the FRAG scheme [5],

$$z = (-n, 2n, -2n, 2n, -2n, n),$$
$$t = (-\tau_1, -\tau_2, -\tau_3, \tau_3, \tau_2, \tau_1).$$

At time $-\tau_1$, n counter-propagating pulse pairs are applied along the trap axis (aligned with the z axis) to provide a $2n\hbar k$ momentum kick in the $-z$ direction.

The GZC scheme [2,4] is characterized as follows:

$$\underline{z} = (-2n, 3n, -2n, 2n, -3n, 2n),$$
$$\underline{t} = (-\tau_1, -\tau_2, -\tau_3, \tau_3, \tau_2, \tau_1).$$

The integer n determines the gate time T_G, which scales optimally with the total number of pulses in the scheme N_p as $T_G \propto N_p^{-2/3}$ [4,6].

The FRAG and GZC schemes consist of $10n$ and $14n$ pulses, respectively. The FRAG scheme has a state-averaged fidelity, as defined in [6], of 0.96 for $n = 1$ and 0.995 for $n = 2$, while for higher n the infidelity is below 10^{-8}. We neglect the low-fidelity $n = 1$ case of the FRAG scheme, which obscures the stability analysis. The GZC scheme, with higher total numbers of pulses for each n, achieves an infidelity of the order of 10^{-5} for $n = 1$ and an infidelity below 10^{-8} for higher n.

The scaling of errors with the number of pulses is examined for both the FRAG and the GZC schemes. We explore the effects of errors on schemes with low pulse numbers using the $n = 1$ GZC scheme due to its high fidelity. While more robust for lower numbers of pulses, the GZC scheme is slower than the FRAG scheme for $n \geqslant 2$, as shown in [5]. The effects of finite laser repetition rates on these schemes are explored in [5,6], where it is shown that for repetition rates of around 300 MHz, even a gate with perfect π pulses has non-negligible infidelity. Faster repetition rates have robust fidelities, particularly for the two-qubit case. Errors due to imperfect pulse areas or from breaking the RWA affect any scheme regardless of repetition rate; in this paper we consider these errors independently by assuming an infinite repetition rate. Furthermore, this approximation allows a clear analysis of the relationship between these errors and the number of applied pulses. The methods in this paper can be applied using particular, finite repetition rates to model the errors in an experiment more precisely.

To model the effect of imperfect pulses or an invalid RWA, we expand the appropriate unitary operator for the applied gate, U_{re}, in the number basis. We can then observe the phase-space evolution during the gate process and calculate the fidelity of the gate. While coherent states are preserved by the momentum kicks and rotations, the momentum kicks deform an initial number state to spread across many modes. At the end of a high-fidelity gate, however, this spread resolves back into the initial number state, as shown in Figs. 1(a)–1(g).

B. Fidelity calculation: Dimensional reduction

To assess the impact of particular errors, we use the state-averaged fidelity as a measure of the gate performance. The fidelity of a pure state $|\psi\rangle$ with respect to a density matrix σ is given by the state overlap [18]:

$$F = \langle\psi|\sigma|\psi\rangle. \tag{7}$$

For an initial state $|\phi_i\rangle$, the final state following the ideal gate operation U_{id} is given by

$$|\psi\rangle = U_{\mathrm{id}}|\phi_i\rangle, \tag{8}$$

and the final density matrix following the real, imperfect, operation U_{re} is given by

$$\sigma = U_{\mathrm{re}}|\phi_i\rangle\langle\phi_i|U_{\mathrm{re}}^\dagger. \tag{9}$$

The state-averaged fidelity is thus

$$F = \int_{\phi_i} |\langle\phi_i|U_{\mathrm{id}}^\dagger U_{\mathrm{re}}|\phi_i\rangle|^2, \tag{10}$$

integrating uniformly over the unit hypersphere described by the initial state with arbitrary coefficients a_{jk}:

$$|\phi_i\rangle = (a_{00}|gg\rangle + a_{01}|ge\rangle + a_{10}|eg\rangle + a_{11}|ee\rangle) \otimes |n_c n_r\rangle. \tag{11}$$

The initial motional state is the number product state $|n_c\rangle \otimes |n_r\rangle$ for the c.m. and stretch modes, respectively. The motional inner product is stricter than the computational fidelity of [6], with the stronger motional restoration requirement that the population must be restored to the initial number state for each mode at the end of the gate operation. This is a convenient choice for our number basis and directly considers effective heating caused by the gate to be infidelity.

The ideal gate operation of Eq. (6), with duration T_G, applies a state-dependent phase while preserving the internal

and motional states:

$$U_{\rm id}|\phi_i\rangle = (e^{i\pi/4}a_{00}|gg\rangle + e^{-i\pi/4}a_{01}|ge\rangle + e^{-i\pi/4}a_{10}|eg\rangle + e^{i\pi/4}a_{11}|ee\rangle) \otimes e^{-iT_G(\nu_c n_c+\nu_r n_r)}|n_c n_r\rangle, \quad (12)$$

where the motional component is global phase, corresponding to free evolution for each mode.

The real gate is a more complex operation on both the computational and the motional states, and we consider the error to first order in the small gate imperfection. Since the ideal gate does not transform the basis states but just applies a phase, a real gate approximating the ideal operation has only small population transfer between internal states. The gate schemes are designed to restore the motional states for preserved internal states; only a fraction of the motional state population (to second order in the error) will be restored for altered internal states with changed state-dependent displacement operators. These terms with changed internal states thus provide a second-order correction to the fidelity, which we neglect here.

Similarly, an ideal counter-propagating pair of pulses acting on two ions with the same internal state affects only the c.m. mode. An imperfect pair of pulses may alter the stretch mode to some small degree: a first-order error term. This perturbation to the stretch mode also has only a small effect on the fidelity; only a fraction of the perturbation is expected to be restored to its initial motional state and this second-order contribution is neglected. Ions with opposite internal states are assumed to have an invariant c.m. mode, with the gate acting on the stretch mode.

For the basis state

$$a_{00}|gg\rangle \otimes |n_c n_r\rangle \equiv a_{00}|ggn_c n_r\rangle, \quad (13)$$

the fidelity inner product element is thus

$$|a_{00}|^2\langle ggn_c|U_{id}^\dagger U_{\rm re}|ggn_c\rangle = |a_{00}|^2 e^{-i\pi/4}\langle ggn_c|U_{\rm re}|ggn_c\rangle, \quad (14)$$

where the stretch mode is allowed to evolve freely by the ideal and real unitaries and, thus, cancels from the inner product. Only the population retained in the computational ground state of both ions is retained in the fidelity term. The unitaries act symmetrically on $|ee\rangle$, and the same symmetry between $|eg\rangle$ and $|ge\rangle$ allows us to simplify our full fidelity expression:

$$F = \int_{\phi_i} |(|a_{00}|^2 + |a_{11}|^2)e^{i\nu_c T_G n_c - i\pi/4}\langle ggn_c|U_{\rm re}|ggn_c\rangle + (|a_{01}|^2 + |a_{10}|^2)e^{i\nu_r T_G n_r + i\pi/4}\langle gen_r|U_{\rm re}|gen_r\rangle|^2. \quad (15)$$

For each internal state of the two qubits, the effect of the real gate on just a single motional mode contributes to the fidelity expression. We thus expand $U_{\rm re}$ for each mode independently and, accordingly, cancel the motional phase term in the ideal unitary from free evolution of the other mode.

A general position operator decomposition for two trapped ions is described by

$$kx_i = b_i^{(c)}\eta_c(a_c + a_c^\dagger) + b_i^{(r)}\eta_r(a_r + a_r^\dagger), \quad (16)$$

where subscript c describes the c.m. mode, and subscript r describes the stretch mode. The coupling operators for two trapped ions are

$$b^{(c)} = \left(\frac{1}{\sqrt{2}}, \frac{1}{\sqrt{2}}\right), \quad (17)$$

$$b^{(r)} = \left(-\frac{1}{\sqrt{2}}, \frac{1}{\sqrt{2}}\right), \quad (18)$$

with the jth vector element representing the coupling for ion j and mode frequencies of ν and $\sqrt{3}\nu$ for the c.m. and stretch modes, respectively.

The real gate unitary $U_{\rm re}$ is applied to both modes, however, to consider first-order errors we can treat it as separable for each mode. This allows us to apply a single-mode expansion of kx_i for each internal state of the qubits. For the states $|gg\rangle$ and $|ee\rangle$, the terms in $U_{\rm re}$ contributing to the fidelity equation, (15), are given by

$$kx_i = b_i^{(c)}\eta_c(a_c + a_c^\dagger), \quad (19)$$

while for $|ge\rangle$ and $|eg\rangle$,

$$kx_i = b_i^{(r)}\eta_r(a_r + a_r^\dagger). \quad (20)$$

Our separable representation of $U_{\rm re}$ reduces the dimension of the state vector by a factor given by the number of required motional basis states. The Hamiltonian is reduced in dimension by the square of this factor. We use the number basis to model the state evolution and truncate the basis such that a negligible population occupies the maximal basis states during the gate operation. This truncation occurs for higher phonon numbers with larger numbers of applied pulses in a gate corresponding to larger momentum kicks. We truncate our number basis at 50 states for $n = 1$ for each gate, 70 states for $n = 2$ and $n = 5$, and 130 states for $n = 10$. The single-mode analysis thus reduces the dimensions for calculating the state vector evolution by a factor of around 100, depending on the number of applied pulses. The state vector's dimension is four times the dimension of the number basis, due to the two basis internal states for each ion.

C. Extending the fidelity calculation to larger traps

Performing fast gates within a large quantum processor requires analysis of gate imperfections in traps with larger numbers of ions. The number of motional modes is equal to the number of trapped ions. The position decomposition can be generalized from Eq. (16) for arbitrary numbers of ions, and we again apply the approximation of separable motional modes in a harmonic trap.

The ideal and real unitaries can be written as a separable product of the operation on each mode,

$$U_{\rm id} = \prod_{p=1}^{L} U_{{\rm id},p}, \quad (21)$$

$$U_{\rm re} = \prod_{p=1}^{L} U_{{\rm re},p}, \quad (22)$$

where L is the number of modes and

$$U_{\mathrm{id},p} = e^{i\phi_p \sigma_1^z \sigma_2^z} \tag{23}$$

up to global phase. This simplifies the fidelity F expression to require only the product of the mode-dependent fidelities F_p up to first order in the error term:

$$F \simeq \int_{\phi_i} |\Pi_p F_p|^2, \tag{24}$$

$$F_p = \langle \phi_i | \, U_{\mathrm{id},p}^{\dagger} U_{\mathrm{re},p} \, | \phi_i \rangle \, . \tag{25}$$

We can calculate the contributions $U_{\mathrm{re},p}$ of each mode to the real gate unitary, using an appropriately truncated single-mode number basis for each calculation. For a high-fidelity gate scheme, the ideal phase contribution for each mode is given by [6]

$$\phi_p = 8\eta_p^2 \sigma_1^z \sigma_2^z b_1^{(p)} b_2^{(p)} \sum_{m=2}^{N} \sum_{k=1}^{m-1} z_m z_k \sin\left(\nu_p (t_m - t_k)\right), \tag{26}$$

where z_k is the number of pulse pairs applied at time t_k determined by the gate scheme. For a high-fidelity gate, $\sum_p \phi_p \approx \frac{\pi}{4}$.

Our method to estimate fidelity in this fashion is to first calculate the real unitaries for each mode $U_{\mathrm{re},p}$ and the ideal phases ϕ_p. The individual mode expansion of the gate unitary ensures a low-dimensional state vector, as required for computation.

III. BREAKING THE RWA

Pulses with a duration of the order of the atomic transition period $2\pi/\omega_{\mathrm{at}}$ render the RWA invalid and cause infidelity in fast gate schemes which rely on the RWA. In this section we apply our fidelity calculation method to explore the trade-off in pulse duration between performing large numbers of pulses in a short time for fast, high-fidelity gates and staying in the regime where the RWA holds. Gates significantly faster than the trap evolution period ($\sim 1\ \mu$s) require large numbers of pulses, which must thus have very short durations. We demonstrate that the valid RWA regime is altered little by the number of applied pulses in a gate.

We perform fast gates using short pulses of varying duration without performing the RWA to investigate the regime where the approximation holds. The gate should also be independent of the optical phase ϕ [19], and we quantify the pulse lengths required for phase independence. In the interaction frame with respect to the internal states of a single ion, ion 1 indicated by subscripts, the atom-light interaction Hamiltonian is

$$H_1' = \frac{\hbar\Omega}{2}(\sigma_1^+ e^{-i(kx_1 - (\omega_L + \omega_{\mathrm{at}})t + \phi)} + \sigma_1^+ e^{i(kx_1 - \delta t + \phi)} + \sigma_1^- e^{-i(kx_1 - \delta t + \phi)} + \sigma_1^- e^{i(kx_1 - (\omega_L + \omega_{\mathrm{at}})t + \phi)}), \tag{27}$$

where $\delta = (\omega_L - \omega_{\mathrm{at}})$. Typical atomic frequency transitions are of the order of $\omega_{\mathrm{at}} \sim 2\pi \times 10^{15}$ Hz, and the fast rotating terms can be neglected following the RWA. Pulse durations are typically assumed to be much longer than the rotation period, $\tau(\pi \times 10^{15}) \gg 1$.

We focus on resonant transitions where $\delta = 0$ for simplicity, such that $\omega_L = \omega_{\mathrm{at}}$. Assuming a constant Ω and a perfect π pulse, such that $\Omega = \pi/\tau$, the unitary operator from Eq. (27) for a single ion is

$$U_{\mathrm{pulse},1} = \exp\left[\frac{-i\pi}{2\tau}\left(\int_{t_i}^{t_f} \sigma_1^+ e^{-i(kx_1 - 2\omega_{\mathrm{at}}t + \phi)} dt + \int_{t_i}^{t_f} \sigma_1^- e^{i(kx_1 - 2\omega_{\mathrm{at}}t + \phi)} dt + \tau\sigma_1^+ e^{i(kx_1 + \phi)} + \tau\sigma_1^- e^{-i(kx_1 + \phi)}\right)\right] \tag{28}$$

for a pulse of duration $\tau = t_f - t_i$, where

$$\int_{t_i}^{t_f} \sigma_1^+ e^{-i(kx_1 - 2\omega_{\mathrm{at}}t + \phi)} dt = \frac{-i\sigma_1^+}{2\omega_{\mathrm{at}}}(e^{-i(kx_1 - 2\omega_{\mathrm{at}}t_f + \phi)} - e^{-i(kx_1 - 2\omega_{\mathrm{at}}t_i + \phi)}). \tag{29}$$

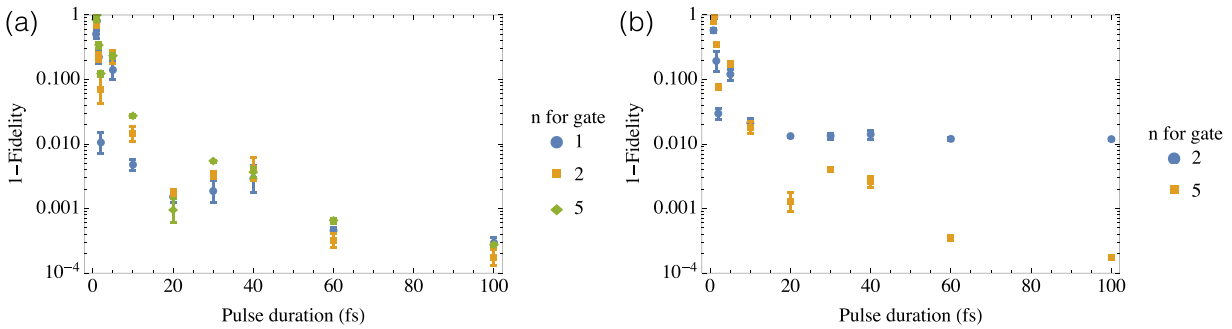

FIG. 2. Infidelity following (a) GZC and (b) FRAG gate operations with different numbers of pulses, governed by n. The effect of changing the duration of the pulses composing the gate is shown. The initial motional state is $|2\rangle_c|2\rangle_r$, the second excited number state for each mode. We determine the mean and the standard deviation (error bars) by varying the phase ϕ for a given pulse duration τ.

For two ions, the interaction Hamiltonian is $H_1' + H_2'$ for ions 1 and 2, using H_i' from Eq. (27). The pulse unitary operator $U_{\text{pulse},1}$ is similarly extended and combined with the motional free evolution unitary, Eq. (5), to construct the real gate unitary U_{re}. This allows us to explore the validity of the RWA for different pulse lengths by solving for the phase dependence and fidelity.

Figure 2 shows the effect of a short pulse duration on the gate fidelity. For a short pulse duration, the fidelity decreases as more pulses are applied for the FRAG and GZC gates. The mean infidelity is plotted for varying phase ϕ, and error bars show the standard deviation in infidelity due to phase dependence. The FRAG gate with $n = 2$ has a fidelity of 0.988 and approaches this value with a standard deviation of less than 10^{-3} for pulse lengths $\tau > 40$ fs. The GZC scheme and the FRAG scheme for $n = 5$ have a fidelity above 0.999 and a standard deviation of less than 10^{-4} for $\tau \geqslant 60$ fs.

Pulses much longer than the atomic transition period are accurately described under the RWA, and the number of pulses in the gate does not significantly alter this threshold. For gates with increasing speed or scalability with the number of ions, large numbers of pulses must be performed much faster than the trap motional frequency, $\nu/(2\pi) \simeq 1$ MHz, or even much faster than 10 ns for momentum application schemes exciting short-lived atomic levels [20]. This provides five orders of magnitude between a safe pulse duration $\sim$100 fs, and the lifetime of typical short-lived levels, such as $P_{3/2}$ in $^{40}Ca^+$.

IV. IMPERFECT PULSES

Significant errors also arise from imperfect π pulses, which construct the momentum kicks fundamental to fast gates. π pulses with an arbitrarily high fidelity can be constructed using composite pulses [21–23]; laser repetition rates must be sufficiently high to accommodate the pulse components in this approach. In this section, we consider the impact of infidelity in the π rotations on the full gate fidelity: both systematic and random errors in the rotations are examined. Imperfect π pulses cause imperfect state transfer, errant momentum kicks, and acquired phase infidelity.

While different methods for performing π pulses have varying robustness to laser fluctuations, the pulse rotation fidelity for any method has a fixed relation to the full gate fidelity. We consider here the simplest case of square pulses to calculate the relation between rotation fidelity and gate fidelity. To model the imperfect gate process, we assume a suitable pulse length for the RWA, with $\delta = 0$:

$$H'_{\text{RWA}} = \frac{\hbar\Omega}{2}(\sigma_+ e^{i(kx+\phi)} + \sigma_- e^{-i(kx+\phi)}). \tag{30}$$

For Ω constant in time, a π pulse satisfies $\Omega\tau = \pi$ for a pulse duration τ. An approximate π pulse satisfies $\Omega\tau = \xi\pi$, with $\xi \simeq 1$. The unitary corresponding to the pulse applied to a single ion follows

$$U_{\text{pulse}} = e^{\frac{-i\xi\pi}{2}(\sigma_+ e^{i(kx+\phi)} + \sigma_- e^{-i(kx+\phi)})}. \tag{31}$$

Reversing the pulse direction changes the sign of k in the evolution operator. The pulse rotation fidelity can be found for ideal and real pulse unitaries U'_{pulse} and U_{pulse}, respectively:

$$\mathcal{F}_{\text{rot}} = \text{Min}_{\psi_i} |\langle\psi_i|(U'_{\text{pulse}})^\dagger U_{\text{pulse}}|\psi_i\rangle|^2 \tag{32}$$

$$\simeq 1 - \frac{(1-\xi)^2\pi^2}{4} \tag{33}$$

up to third order in $(1-\xi)\pi/2$.

Assuming that the same laser produces each pulse, and that phase drift is minimal during the gate duration (<1 μs), ϕ is fixed. The unitary for a counter-propagating pulse pair, with first pulse direction z, can be expressed in the computational basis $\{e,g\}$,

$$U_{\text{pair}}(z,\xi) = \begin{pmatrix} e^{-izkx}(\cos(kx)\cos(\pi\xi) + iz\sin(kx)) & \cos(kx)\sin(\pi\xi)(-i\cos(\phi) + \sin(\phi)) \\ \cos(kx)\sin(\pi\xi)(-i\cos(\phi) - \sin(\phi)) & e^{izkx}(\cos(kx)\cos(\pi\xi) - iz\sin(kx)) \end{pmatrix}, \tag{34}$$

such that $\xi = 1$ gives

$$U_{\text{pair}}(z,1) = -\begin{pmatrix} e^{-2izkx} & 0 \\ 0 & e^{2ikx} \end{pmatrix}, \tag{35}$$

with the expected state-dependent momentum kicks and no ϕ dependence. The ϕ dependence for imperfect pulses is in the terms of Eq. (34), corresponding to population transfer between internal states, and represents the angle of rotation on the Bloch sphere. It does not affect the magnitude of rotation, which provides the error, and we set $\phi = 0$ for simplicity.

The motional and internal operators commute for separate ions, and the unitary for a two-ion imperfect π pulse is given by

$$U_{2\text{pulse}}(z) = e^{\frac{-i\xi\pi}{2}(\sigma_1^+ e^{izkx_1} + \sigma_1^- e^{-izkx_1} + \sigma_2^+ e^{izkx_2} + \sigma_2^- e^{-izkx_2})}. \tag{36}$$

Using this unitary we construct the evolution from pulse pairs, which we intersperse with the motional free evolution unitaries to build up our gate operations. The necessary pulse times for gates with varying numbers of pulses are found according to the applied scheme [2,6].

A. Systematic errors

First, we fix ξ to be constant during a gate operation to find the systematic error effects. Figure 3 shows the effect of the initial motional state on the final mode occupation and gate fidelity for a GZC gate with $n = 1$. Increasing infidelity in individual π pulses, or rotation infidelity, damages the full gate fidelity and increases both the mean and the standard deviation of the mode occupation after the gate. The initial motional state before the gate is applied affects the magnitude of the gate infidelity. There is not a clear relationship between initial motional state and infidelity; however, each initial

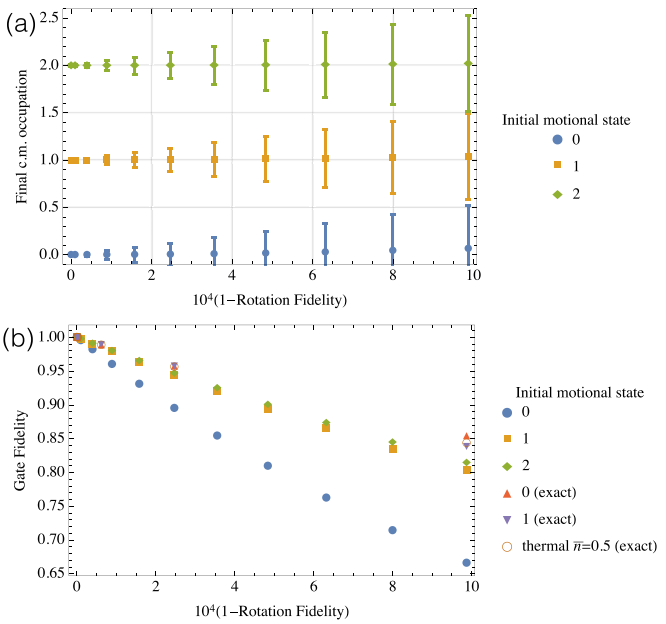

FIG. 3. A GZC gate with $n = 1$ is applied with varying rotation infidelity (1 − fidelity) for individual pulses and different initial motional occupation. (a) The mean and standard deviation (error bars) of the occupation of motional number states following the gate. (b) The gate fidelity is calculated as a function of the pulse rotation fidelity for initial number states (0, 1, and 2) using the fidelity lower-bound method. The exact fidelity is calculated for both the ground and the first excited number states (0 and 1, exact) and a thermal state with mean phonon number $\bar{n} = 0.5$ for comparison, using a representative internal state.

state is harmed by pulse errors. A rotation infidelity around 3×10^{-4} is required for a gate fidelity better than 0.9, or a rotation infidelity around 10^{-5} for a gate fidelity above 0.99. These values clearly provide a lower bound in the figure: the exact fidelity calculations for the thermal, ground, and first excited motional states have less stringent requirements. The ground-state approximate fidelity calculation provides a bound significantly lower than its exact value, while the approximate first excited state provides a more typical, much closer bound to its exact counterpart. For tractable calculation, exact fidelities here are using a representative internal state $\frac{1}{2}(|00\rangle + |01\rangle + |10\rangle + |11\rangle)$, which captures the full motional dynamics of the gate, in place of the state-averaged fidelity.

It is important to note that the fidelity calculation method outlined in Sec. II is directly applicable only for pure motional states. This is due to the more complex form of the fidelity for mixed states and resulting issues in separating component motional mode and internal state evolution as in our fidelity approximation method. In Fig. 3(b), the exact fidelity calculation (without approximation) is performed using a representative internal state for both thermal and number motional states. Here we examine a thermal state with a mean phonon number $\bar{n} = 0.5$ for both motional modes; initial states with mean phonon number $\bar{n}$ much lower than 0.5 have been prepared, for example, near ground-state cooling ($\bar{n} < 0.05$) in [17,24]. This thermal state has projections of 0.67, 0.22, and 0.07 onto the ground, first, and second excited number states, respectively; these number states are expected to provide a strong indication of the thermal-state fidelity. Indeed, the exact fidelity calculations for the ground and first excited number states are nearly identical to the exact thermal-state fidelity

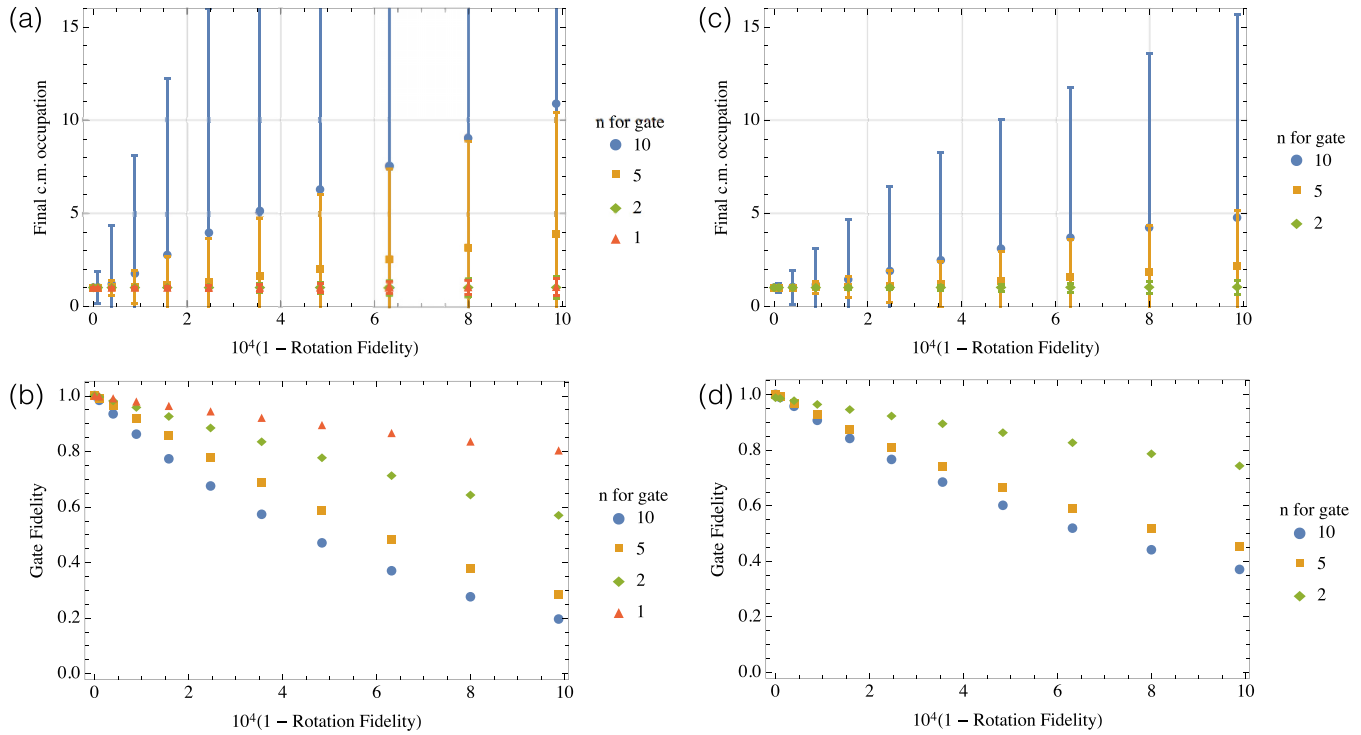

FIG. 4. (a, b) GZC and (c, d) FRAG fast gates are applied to $|ee\rangle|1\rangle_c|1\rangle_r$ with varying n and pulse rotation error. (a, c) The mean and standard deviation (error bars) of the occupation of the c.m. mode are shown following the gate applied to the $|ee\rangle$ internal state. (b,d) The gate fidelity is shown as a function of the pulse rotation infidelity.

calculation, and the fidelity calculations to first order in the imperfection for each initial number state provide a lower bound for the full thermal-state fidelity calculation.

Higher numbers of perfect π pulses provide faster gate times, more stability, and improved scalability. However, as the number of pulses in the gate increases with n, the errors in each pulse cause compounding gate infidelities, shown in Fig. 4. For both the FRAG and the GZC gates, Fig. 4 shows dramatic increases in the mean and standard deviation of the motional state following a gate as the number of pulses increases. For each scheme, with $n \lesssim 10$, a rotation infidelity of less than 10^{-5} is required for a gate fidelity above 0.99, or a rotation infidelity of less than 10^{-4} is required for a gate fidelity above 0.9. Both schemes are similarly affected by pulse error compounding with pulse number.

Using square pulses, where the pulse area is proportional to ξ, we can find the pulse-area stability requirements. Systematic pulse area error $(1-\xi)$ of the order of 0.4% is permissible for a fidelity better than 0.9 and $n \lesssim 10$ for each scheme. A pulse-area error $(1-\xi) \leqslant 0.2\%$ is required for a fidelity above 0.98. Figure 5 demonstrates the impact of systematic pulse-area errors on the internal state and mode occupation following a GZC gate with $n = 1$; population is lost to other internal states with variable motional mode occupation.

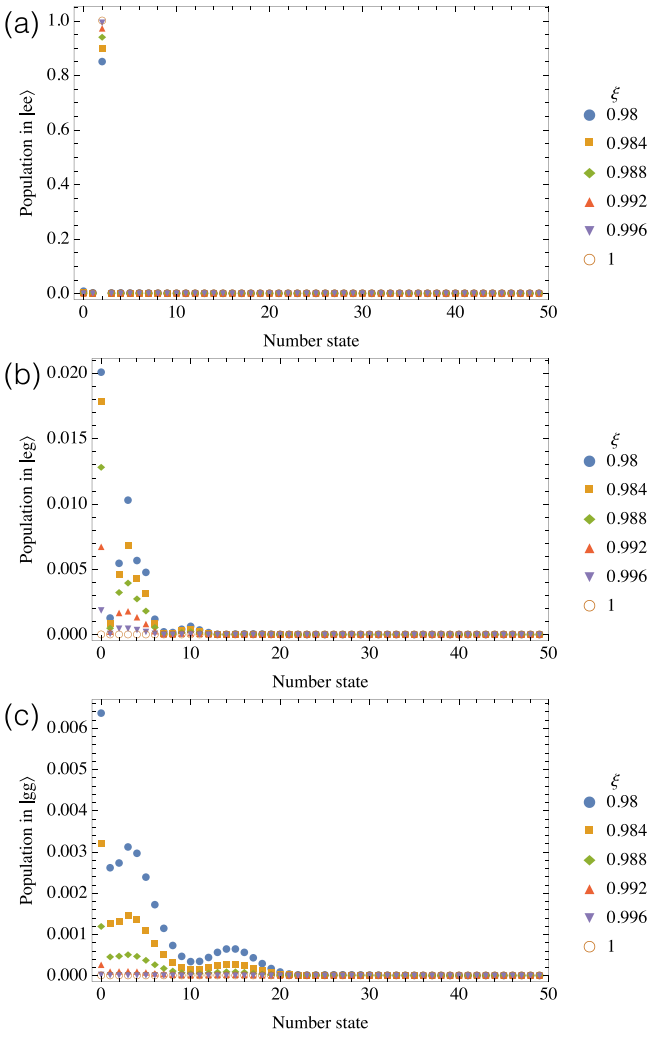

FIG. 5. Population in the (a) $|ee\rangle$, (b) $|eg\rangle$, and (c) $|gg\rangle$ states for different c.m. number states after a GZC gate applied to $|ee\rangle \otimes |2\rangle_c$ with $n = 1$. The fraction ξ of a perfect square π pulse performed determines the restoration of the internal state and c.m. motional mode to the initial state.

B. Random errors

We now consider the effects of random fluctuations in the laser intensity, which give rise to corresponding fluctuations in the pulse area parameter ξ. These fluctuations typically approximate a Gaussian, and we construct our gate unitary from pulse pairs with a random ξ parameter randomly sampled from a Gaussian distribution. Each pulse in a given pair is chosen to have the same area modifier ξ, as the pairs are assumed to be constructed from a single laser pulse divided by a beam splitter.

Figure 6 demonstrates the effect of random errors on a particular gate fidelity. This histogram shows the fidelities for a GZC gate with 14 pulse pairs ($n = 1$), where the pulse-area fluctuations obey a Gaussian distribution with standard deviation 0.02. For 300 gate calculations with fluctuations in the pulse areas, the gate fidelities form the distribution shown in the figure.

As for systematic errors in the pulse area, different initial motional states give rise to similar fidelities, while the number of applied pulses has a much more significant trend as shown in Fig. 7. For a given standard deviation for pulse-area fluctuations, more applied pulses give rise to larger errors in a gate as the rotation errors compound. Larger fluctuations, represented by a larger standard deviation in the pulse-area distribution, similarly give rise to lower gate fidelities. As each gate fidelity is sampling from a distribution, as shown in Fig. 6, Fig. 7 shows the mean fidelity and standard deviation (error bars) for each gate fidelity distribution. The results for random pulse intensities are comparable to the systematic error results: Fig. 7(b) shows the relationship between the standard deviation in the pulse area and the mean rotational infidelity. Random fluctuations in the pulse area give rise to variable rotational fidelities, which can compensate for errors in separate pulse

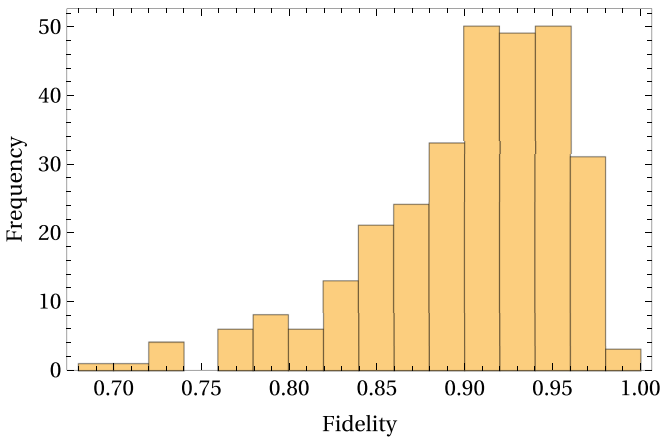

FIG. 6. Fast gate fidelity distribution for 300 runs of a GZC gate ($n = 1$) with random pulse-area fluctuations according to a Gaussian distribution with standard deviation 0.02. The ions are initially in the first excited state of each motional mode.

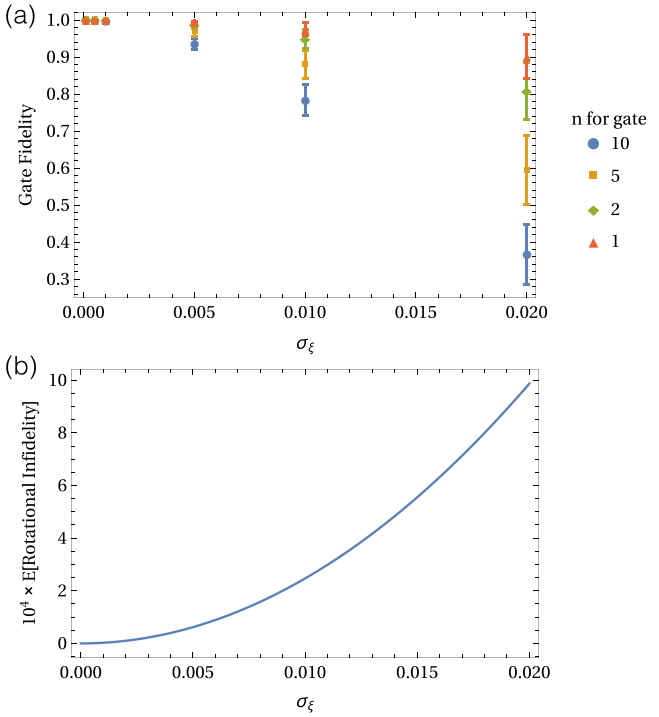

FIG. 7. (a) GZC gate fidelities for varying n with Gaussian fluctuations in the pulse area with varying standard deviation in ξ (σ_ξ). The initial motional states are in the first excited number state for each mode. Error bars correspond to the standard deviation of the gate fidelity distribution. (b) The relationship between σ_ξ and the mean rotational infidelity are shown for comparison with systematic error results.

pairs and provide higher average gate fidelities than in the systematic case.

V. CONCLUSIONS

The duration of fast gates directly impacts their fidelity and scalability with the number of trapped ions; sufficiently fast gate schemes are relatively invariant with the number of trapped ions [6,11]. We have presented a technique for calculating gate fidelities to first order in the error for large numbers of applied pulses. Applying this technique to two ions, we have demonstrated that pulse errors cause compounding infidelity with the number of pulses composing the gate. The gate duration scales with the number of pulses, so this pulse fidelity requirement is of great importance for using fast gates for scalable QIP. A pulse infidelity of less than 10^{-5} is required for a gate fidelity above 0.99 with up to 140 pulse pairs in the FRAG and GZC gate schemes. We have also shown that different numbers of applied pulses do not significantly alter the valid RWA regime: pulse durations much longer than the atomic transition period are required. Experimental implementation of a fast gate, which requires fast and robust π pulses, will be a significant step towards large-scale QIP with ions.

ACKNOWLEDGMENTS

This work was supported by the Australian Research Council Centre of Excellence for Quantum Computation and Communication Technology (Project No. CE110001027) (A.R.R.C.), the Australian Research Council Future Fellowship (FT120100291) (J.J.H.), and Australian Research Council Discovery Project No. DP130101613 (J.J.H., A.R.R.C.).

[1] D. P. DiVincenzo, The physical implementation of quantum computation, Fortschr. Phys. **48**, 771 (2000).
[2] J. J. García-Ripoll, P. Zoller, and J. I. Cirac, Speed Optimized Two-Qubit Gates with Laser Coherent Control Techniques for Ion Trap Quantum Computing, Phys. Rev. Lett. **91**, 157901 (2003).
[3] L.-M. Duan, Scaling ion trap quantum computation through fast quantum gates, Phys. Rev. Lett. **93**, 100502 (2004).
[4] J. García-Ripoll, P. Zoller, and J. Cirac, Coherent control of trapped ions using off-resonant lasers, Phys. Rev. A **71**, 062309 (2005).
[5] C. D. B. Bentley, A. R. R. Carvalho, D. Kielpinski, and J. J. Hope, Fast gates for ion traps by splitting laser pulses, New J. Phys. **15**, 043006 (2013).
[6] C. D. B. Bentley, A. R. R. Carvalho, and J. J. Hope, Trapped ion scaling with pulsed fast gates, New J. Phys. **17**, 103025 (2015).
[7] J. Mizrahi, B. Neyenhuis, K. G. Johnson, W. C. Campbell, C. Senko, D. Hayes, and C. Monroe, Quantum control of qubits and atomic motion using ultrafast laser pulses, Appl. Phys. B **114**, 45 (2014).
[8] S.-L. Zhu, C. Monroe, and L.-M. Duan, Trapped ion quantum computation with transverse phonon modes, Phys. Rev. Lett. **97**, 050505 (2006).
[9] G.-D. Lin, S.-L. Zhu, R. Islam, K. Kim, M.-S. Chang, S. Korenblit, C. Monroe, and L.-M. Duan, Large-scale quantum computation in an anharmonic linear ion trap, Europhys. Lett. **86**, 60004 (2009).
[10] P. Zou, J. Xu, W. Song, and S.-L. Zhu, Implementation of local and high-fidelity quantum conditional phase gates in a scalable two-dimensional ion trap, Phys. Lett. A **374**, 1425 (2010).
[11] S.-L. Zhu, C. Monroe, and L.-M. Duan, Arbitrary-speed quantum gates within large ion crystals through minimum control of laser beams, Europhys. Lett. **73**, 485 (2006).
[12] M. Petrasiunas, M. Hussain, J. Canning, M. Stevenson, and D. Kielpinski, Picosecond 554 nm yellow-green fiber laser source with average power over 1 W, Opt. Express **22**, 17716 (2014).
[13] W. C. Campbell, J. Mizrahi, Q. Quraishi, C. Senko, D. Hayes, D. Hucul, D. N. Matsukevich, P. Maunz, and C. Monroe, Ultrafast Gates for Single Atomic Qubits, Phys. Rev. Lett. **105**, 090502 (2010).
[14] J. Mizrahi, C. Senko, B. Neyenhuis, K. G. Johnson, W. C. Campbell, C. W. S. Conover, and C. Monroe, Ultrafast Spin-Motion Entanglement and Interferometry with a Single Atom, Phys. Rev. Lett. **110**, 203001 (2013).
[15] M. A. Nielsen and I. L. Chuang, *Quantum Computation and Quantum Information* (Cambridge University Press, Cambridge, 2000).
[16] E. Knill, Quantum computing with realistically noisy devices, Nature **434**, 39 (2005).

[17] J. Benhelm, G. Kirchmair, C. F. Roos, and R. Blatt, Towards fault-tolerant quantum computing with trapped ions, Nat. Phys. **4**, 463 (2008).

[18] A. Gilchrist, N. Langford, and M. Nielsen, Distance measures to compare real and ideal quantum processes, Phys. Rev. A **71**, 062310 (2005).

[19] A. M. Steane, G. Imreh, J. P. Home, and D. Leibfried, Pulsed force sequences for fast phase-insensitive quantum gates in trapped ions, New J. Phys. **16**, 053049 (2014).

[20] R. Gerritsma, G. Kirchmair, F. Zähringer, J. Benhelm, R. Blatt, and C. F. Roos, Precision measurement of the branching fractions of the $4p\,2P_{3/2}$ decay of Ca II, Eur. Phys. J. D **50**, 13 (2008).

[21] B. T. Torosov and N. V. Vitanov, Smooth composite pulses for high-fidelity quantum information processing, Phys. Rev. A **83**, 053420 (2011).

[22] S. S. Ivanov and N. V. Vitanov, High-fidelity local addressing of trapped ions and atoms by composite sequences of laser pulses, Opt. Lett. **36**, 1275 (2011).

[23] I. Cohen, A. Rotem, and A. Retzker, Phys. Rev. A **93**, 032340 (2016).

[24] C. J. Ballance, T. P. Harty, N. M. Linke, M. A. Sepiol, and D. M. Lucas, arXiv:1512.04600.